



**Extending Surface Enhanced Raman Spectroscopy (SERS) of  
Atmospheric Aerosol Particles to the Accumulation Mode  
(150-800 nm)**

Journal:	<i>Environmental Science: Processes &amp; Impacts</i>
Manuscript ID	EM-ART-06-2018-000276.R1
Article Type:	Paper
Date Submitted by the Author:	03-Aug-2018
Complete List of Authors:	Tirella, Peter; University of Michigan Department of Chemistry, Chemistry Craig, Rebecca; University of Michigan Department of Chemistry, Chemistry Tubbs, Darrell; University of Michigan Department of Chemistry, Chemistry Olson, Nicole; University of Michigan Department of Chemistry, Chemistry Lei, Ziyang; University of Michigan School of Public Health, Environmental Health Sciences Ault, Andrew; University of Michigan, Environmental Health Sciences

### Environmental Significance Statement

Aerosols act as a surface for heterogeneous reactions and multiphase processes in the atmosphere, which impacts their climate-relevant properties (scattering, absorption, and cloud droplet and ice crystal nucleation). Raman microspectroscopy is able to probe organic and inorganic functional groups at ambient temperature and pressure, but is challenging to apply to aerosols critical to climate since the most abundant sizes by number in the atmosphere (~100 nm) are smaller than the diffraction limit of visible light. We show that surface enhanced Raman spectroscopy (SERS) can extend analysis of atmospheric particles down to 150 nm, revealing new chemical detail about accumulation mode particles in the atmosphere and the potential to enable future studies of the complex chemistry occurring at aerosol surfaces.

1  
2  
3 **1 Extending Surface Enhanced Raman Spectroscopy (SERS) of Atmospheric Aerosol**  
4 **2 Particles to the Accumulation Mode (150-800 nm)**  
5 **3**

6 **4 Peter N. Tirella<sup>1</sup>, Rebecca L. Craig<sup>1</sup>, Darrell B. Tubbs<sup>1</sup>, Nicole E. Olson<sup>1</sup>, Ziyang Lei<sup>2</sup>, Andrew**  
7 **5 P. Ault<sup>1,2\*</sup>**  
8 **6**

9 **7 <sup>1</sup>Department of Chemistry, University of Michigan, Ann Arbor, Michigan, 48109**

10 **8 <sup>2</sup>Department of Environmental Health Sciences, University of Michigan, Ann Arbor, Michigan,**  
11 **9 48109**

12 **10**  
13 **11**  
14 **12 \*corresponding author's e-mail: [aulta@umich.edu](mailto:aulta@umich.edu)**  
15 **13**  
16  
17  
18  
19  
20  
21  
22  
23  
24  
25  
26  
27  
28  
29  
30  
31  
32  
33  
34  
35  
36  
37  
38  
39  
40  
41  
42  
43  
44  
45  
46  
47  
48  
49  
50  
51  
52  
53  
54  
55  
56  
57  
58  
59  
60

1  
2  
3 14 **Abstract (50-250 words)**  
4

5 15 Due to their small size, measurements of the complex composition of atmospheric  
6  
7 16 aerosol particles and their surfaces are analytically challenging. This is particularly true for  
8  
9 17 microspectroscopic methods, where it can be difficult to optically identify individual particles  
10  
11 18 smaller than the diffraction limit of visible light (~350 nm) and measure their vibrational modes.  
12  
13 19 Recently, surface enhanced Raman spectroscopy (SERS) has been applied to the study of aerosol  
14  
15 20 particles, allowing for detection and characterization of previously undistinguishable vibrational  
16  
17 21 modes. However, atmospheric particles analyzed via SERS have primarily been > 1  $\mu\text{m}$  to date,  
18  
19 22 much larger than the diameter of the most abundant atmospheric aerosols (~100 nm). To push  
20  
21 23 SERS towards more relevant particle sizes, a simplified approach involving Ag foil substrates  
22  
23 24 was developed. Both ambient particles and several laboratory-generated model aerosol systems  
24  
25 25 (polystyrene latex spheres (PSLs), ammonium sulfate, and sodium nitrate) were investigated to  
26  
27 26 determine SERS enhancements. SERS spectra of monodisperse, model aerosols between 400-  
28  
29 27 800 nm were compared with non-SERS enhanced spectra, yielding average enhancement factors  
30  
31 28 of  $10^2$  for both inorganic and organic vibrational modes. Additionally, SERS-enabled detection  
32  
33 29 of 150 nm size-selected ambient particles represent the smallest individual aerosol particles  
34  
35 30 analyzed by Raman microspectroscopy to date, and the first time atmospheric particles have been  
36  
37 31 measured at sizes approaching the atmospheric number size distribution mode. SERS-enabled  
38  
39 32 detection and identification of vibrational modes in smaller, more atmospherically-relevant,  
40  
41 33 particles has the potential to improve understanding of aerosol composition and surface  
42  
43 34 properties, as well as their impact on heterogeneous and multiphase reactions involving aerosol  
44  
45 35 surfaces.  
46  
47  
48  
49  
50  
51  
52  
53  
54  
55  
56  
57  
58  
59  
60

## 1 Introduction

Atmospheric aerosol particles impact climate by scattering and absorbing solar radiation and acting as cloud condensation and ice nuclei, which modify cloud properties and precipitation.<sup>1-8</sup> However, these impacts are difficult to quantify due to the complex physicochemical properties of aerosols,<sup>8-10</sup> particularly in terms of chemical composition and mixing state.<sup>9,11-19</sup> This is complicated by the fact that individual particles can contain hundreds to thousands of different chemical species from different sources and atmospheric aging.<sup>8</sup> An important example of aerosol chemical complexity is secondary organic aerosol (SOA), which forms when low volatility oxidation products of volatile organic compounds (VOCs) condense onto or heterogeneously react with existing aerosol particles containing inorganic salts (e.g. ammonium sulfate).<sup>20-22</sup> Though it is known that these particles contain both organic and inorganic components, particle-to-particle variability in chemical composition and mixing state due to different multiphase processes in the atmosphere are not well understood.<sup>20,23,24</sup> In addition, aerosols can have intraparticle chemical variability through processes such as liquid-liquid phase separations.<sup>24-28</sup> More detailed investigations of particle chemical composition and surface properties are needed to improve understanding of multiphase processes,<sup>29,30</sup> such as heterogeneous reactions occurring on surfaces,<sup>31-33</sup> water uptake,<sup>34,35</sup> viscous particles,<sup>36-38</sup> phase transitions,<sup>39,40</sup> and gas-particle partitioning.<sup>41,42</sup>

Over the past decade, Raman microspectroscopy has been increasingly applied as an analytical technique for chemical characterization of aerosol particles.<sup>9,43-46</sup> This technique uses inelastically scattered light to detect vibrational modes present within a sample, which can then be used to identify functional groups and chemical species. Raman microspectroscopy has been applied to characterize many different particle types, such as sea spray and other marine

1  
2  
3 59 aerosol,<sup>44,47-49</sup> soot and elemental carbon (EC) particles,<sup>50-53</sup> mineral dust,<sup>53-56</sup> and SOA,<sup>46</sup> as  
4  
5 60 well as specific compounds commonly found in aerosols, including biological molecules<sup>57</sup> and  
6  
7 61 various organic compounds like organic nitrates,<sup>58</sup> organosulfates,<sup>59</sup> and glyoxal oligomers.<sup>60</sup>  
8  
9  
10 62 Raman analysis has also been used to study hygroscopic properties,<sup>61-65</sup> phase separations,<sup>66-68</sup>  
11  
12 63 heterogeneous reactions,<sup>49,69,70</sup> ice nucleation,<sup>71</sup> and acidity of aerosols.<sup>72,73</sup> Advantages of this  
13  
14 64 technique include minimal sample preparation and non-destructive analysis under ambient  
15  
16 65 temperature and relative humidity (RH) conditions. However, detection limits in terms of both  
17  
18 66 particle size and analyte concentrations can make Raman microspectroscopic studies of aerosol  
19  
20 67 particles challenging. The majority of aerosol particles, particularly those with long atmospheric  
21  
22 68 lifetimes that react and undergo atmospheric processing, are smaller than 1  $\mu\text{m}$ , but Raman  
23  
24 69 microspectroscopy has been applied mostly to the study of individual particles larger than 1  $\mu\text{m}$ ,  
25  
26 70 often 10-30  $\mu\text{m}$ , because it is difficult to optically distinguish smaller particles due to the  
27  
28 71 wavelengths commonly used for Raman analysis (532 or 640 nm) and the diffraction limit of  
29  
30 72 optical microscopy (300-400 nm). Furthermore, even in supermicron atmospheric particles,  
31  
32 73 chemical species are often present in very low concentration, making it difficult to detect Raman  
33  
34 74 signal with enough intensity to determine the identity of vibrational modes and corresponding  
35  
36 75 functional groups. Lastly, important particle properties, such as deliquescence relative humidity  
37  
38 76 can be size-dependent, limiting the ability to translate studies on large particles to  
39  
40 77 atmospherically relevant sizes.<sup>74</sup> If SERS can be used to overcome the detection limit challenges  
41  
42 78 associated with small particle sizes, the potential for Raman microspectroscopic analysis of  
43  
44 79 aerosol particles to improve understanding of chemical composition and mixing state will greatly  
45  
46 80 increase.  
47  
48  
49  
50  
51  
52  
53  
54  
55  
56  
57  
58  
59  
60

1  
2  
3 81 Surface enhanced Raman spectroscopy (SERS) has been used to improve the limit of  
4  
5 82 detection of low concentration chemical species,<sup>75</sup> all the way to single molecules.<sup>76</sup> Through  
6  
7  
8 83 SERS, weak Raman signals are enhanced via interactions with localized surface plasmon  
9  
10 84 resonances (LSPRs), which are generated by excited electrons in metallic substrates.<sup>75,77–80</sup> The  
11  
12 85 metallic substrates are often silver, gold, or copper and can be in the form of foils, geometric  
13  
14 86 nanoparticles, and colloids.<sup>78,80,81</sup> SERS has applications in many different fields, from  
15  
16  
17 87 biosensing to art preservation, and enhancement factors (EFs) for vibrational intensities of  
18  
19 88 analytes are reported that range from  $10^2 - 10^{10}$ .<sup>75,77–80,82,83</sup> The volumes that experience SERS  
20  
21 89 enhancements are small and typically located less than 5-10 nm from a hotspot, which shows the  
22  
23  
24 90 potential to measure submicron particles that are challenging to identify optically, since a  
25  
26 91 detected SERS-enhanced spectrum originates from a such a small area, it most likely  
27  
28 92 corresponds to an individual particle at low substrate loadings (e.g. no particle overlap). In the  
29  
30  
31 93 future, SERS hotspots could be used to probe phenomena localized near aerosol surfaces. With  
32  
33 94 SERS, limitations of optically distinguishing particles for analysis and detection of chemical  
34  
35 95 species present in trace amounts within aerosol particles can be overcome.

36  
37  
38 96 Prior to 2015, only a few preliminary, qualitative studies had used SERS for aerosol  
39  
40 97 analysis, with a focus on bioaerosols.<sup>84–86</sup> Since 2015, SERS has been applied to the study of  
41  
42 98 aerosol particles more broadly and in a more quantitative manner. In 2015, Craig et al. used  
43  
44 99 silver nanoparticle coated quartz substrates to investigate both ammonium sulfate and sodium  
45  
46  
47 100 nitrate aerosol particle standards as well as ambient aerosol.<sup>87</sup> In 2016, Fu et al. used Klarite, a  
48  
49 101 commercially available Au substrate of structured gold inverted pyramids, to study mixed  
50  
51 102 ammonium sulfate and naphthalene particles.<sup>88</sup> A few variations of SERS, such as tip-enhanced  
52  
53  
54 103 Raman spectroscopy (TERS),<sup>89</sup> electrospray SERS (ES-SERS),<sup>90</sup> and surface-enhanced

1  
2  
3 104 resonance Raman spectroscopy (SERRS) of trapped and suspended particles,<sup>91</sup> have also been  
4  
5 105 applied to study aerosol particles. Reported EFs ranged from 2.0 – 70 for  $\nu_s(\text{SO}_4^{2-})$ ,  $\nu_s(\text{NO}_3^-)$ ,  
6  
7 106  $\nu(\text{C-H})$ ,  $\nu(\text{O-H})$ , and  $\delta(\text{C-C})$  vibrational modes<sup>87,88,90</sup> and  $10^5$  for vibrational modes of  
8  
9  
10 107 Rhodamine 590 chloride (R6G), a dye with a large scattering cross-section commonly used for  
11  
12 108 SERS studies.<sup>91</sup> However, most particles probed in these studies were supermicron, not in the  
13  
14 109 submicron size range most abundant for ambient aerosol, and further work is needed to increase  
15  
16 110 EFs for vibrational modes corresponding to more atmospherically-relevant chemical compounds.  
17  
18

19 111 In this study, silver SERS substrates, including Ag nanoparticles and commercial Ag foil,  
20  
21 112 were tested with both organic and inorganic species commonly observed in aerosols.  
22  
23 113 Additionally, laboratory-generated and ambient aerosol particles  $<1 \mu\text{m}$  were analyzed to explore  
24  
25 114 the lower limit in terms of particle size for SERS using these simple methods. The results of this  
26  
27 115 study highlight the potential for SERS analysis of aerosol particles with atmospherically-relevant  
28  
29 116 sizes (down to 150 nm) to improve understanding of chemical composition, mixing state, and  
30  
31 117 reactions occurring on aerosol surfaces that impact aerosol climate effects.  
32  
33

## 34 118 **2 Experimental**

### 35 119 **2.1 Materials and Reagents**

36 120 Quartz slides (Ted Pella, Inc.) and silver foil (ESPI Metals) were purchased and used as  
37  
38 121 substrates. Silver nitrate ( $\text{Ag}(\text{NO}_3)_2$ ) (Sigma-Aldrich), hydroxylamine hydrochloride (Sigma-  
39  
40 122 Aldrich), and sodium hydroxide (Fischer) were used for silver nanoparticle (AgNP) synthesis  
41  
42 123 (described below). Polystyrene latex sphere (PSL) standards (Polysciences, Inc.), ammonium  
43  
44 124 sulfate ( $(\text{NH}_4)_2\text{SO}_4$ ) (Alfa Aesar), and sodium nitrate (Sigma Aldrich) were used as model  
45  
46 125 aerosol systems. All chemicals were  $>98\%$  purity and used without further purification.  
47  
48  
49  
50  
51  
52

### 53 126 **2.2 Substrate Preparation**



1  
2  
3 127 Quartz coverslips were cut and cleaned prior to use as either directly as substrates or as a  
4  
5 128 base for a silver nanoparticle (AgNP) SERS substrates. AgNPs were synthesized by reducing  
6  
7 129 silver nitrate with hydroxylamine hydrochloride, according to the method by Leopold and  
8  
9  
10 130 Lendl.<sup>92</sup> The resulting colloidal solution of AgNPs was drop-coated onto clean quartz slides and  
11  
12 131 dried in a desiccator to create SERS substrates in the same manner as Craig et al.<sup>87</sup> Size  
13  
14 132 distribution data collected via Nanoparticle Tracking Analysis (NTA)<sup>93–95</sup> for the AgNPs prior to  
15  
16  
17 133 dropcoating is included in the Supplementary Information. Silver foil (0.002” thick, ESPI  
18  
19 134 Metals) was cut for use as SERS substrates. Microscopy characterization of the Ag foil is  
20  
21 135 included in the Supplementary Information.

### 24 136 **2.3 Laboratory-Generated Aerosol Particle Samples**

26 137 Organic particle standards were generated by aerosolizing colloidal solutions of PSLs of  
27  
28 138 varying size (400 nm, 600 nm, and 800 nm). Prior studies have analyzed PSLs with SERS going  
29  
30 139 back to the 1990’s,<sup>96</sup> providing useful reference points for Raman studies focused on aerosol  
31  
32  
33 140 particles. Inorganic aerosol particle standards were generated by aerosolizing solutions of 30 mM  
34  
35 141 (NH<sub>4</sub>)<sub>2</sub>SO<sub>4</sub> or 30 mM NaNO<sub>3</sub>. All solutions were made with 18.3 MΩ Milli-Q water.  
36  
37 142 Aerosolization was conducted with a Collison nebulizer operated with HEPA-filtered air and the  
38  
39 143 generated aerosol was passed through two diffusion dryers to remove excess water before being  
40  
41  
42 144 impacted onto substrates with a microanalysis particle sampler (MPS-3, California Instruments,  
43  
44 145 Inc.). Prior to impaction, the inorganic standard particles were size-selected at 400 nm, 600 nm,  
45  
46 146 or 800 nm (electrical mobility diameter) with an electrostatic classifier (Model 3080, TSI  
47  
48 147 Corporation) equipped with a long differential mobility analyzer (Model 3082, TSI Corporation)  
49  
50 148 at sample to sheath flow ratio of 1:8.3 (0.3 to 2.5 lpm)

### 54 149 **2.4 Ambient Aerosol Particle Samples**

1  
2  
3 150 Ambient samples were collected from outside the University of Michigan Chemistry  
4  
5 151 Building (42.2783° N, 83.7372° W). Samples were size selected at 150 nm (electrical mobility  
6  
7 152 diameter) with an electrostatic classifier (Model 3080, TSI Corporation) and then collected on  
8  
9 153 Ag foil via impaction with the MPS-3. Each sample was collected for ~1 hour.

## 12 154 **2.5 Raman Microspectroscopy**

14 155 Raman analysis was performed with a Horiba Labram HR Evolution Raman spectrometer  
15  
16 156 (Horiba Scientific) coupled to a confocal optical microscope (100x Olympus objective, 0.9  
17  
18 157 N.A.). The spectrometer was equipped with a Nd:YAG laser source (50mW, 532nm) and a CCD  
19  
20 158 detector. A 600 groove/mm diffraction grating yielded spectral resolution of 1.8 cm<sup>-1</sup>.  
21  
22 159 Calibration was carried out daily against the Stokes Raman signal of a pure silicon standard at  
23  
24 160 520 cm<sup>-1</sup>. Laser power was attenuated with neutral density (ND) filters ranging from 1 to 100 to  
25  
26 161 prevent sample damage. Spectra were collected for the range of 500 to 4000 cm<sup>-1</sup> for 3  
27  
28 162 accumulations with 15 s acquisition time. 8-15 particles were analyzed for each sample. Raman  
29  
30 163 maps were collected with computer-controlled XY Raman mapping, with spectra recorded using  
31  
32 164 a point-by-point scanning mode with a 0.25 μm step size. Map spectra were also collected from  
33  
34 165 500 to 4000 cm<sup>-1</sup> for 3 accumulations with 15 s acquisition time. Each spectrum collected during  
35  
36 166 a map acquisition was matched to its corresponding location in an optical image to determine if it  
37  
38 167 represented an aerosol particle. Samples were exposed to ambient relative humidity and  
39  
40 168 temperature conditions during Raman analysis (~23°C and 40-60% RH).

41  
42 169 SERS EFs were calculated for vibrational modes of interest according to Equation 1,  
43  
44 170  $I_{\text{SERS}}$  and  $I_{\text{RS}}$  are the Raman signal under SERS and non-SERS conditions, respectively, and  $c_{\text{SERS}}$   
45  
46 171 and  $c_{\text{RS}}$  are the analyte concentration under SERS and non-SERS conditions, respectively.<sup>97</sup>

47  
48  
49  
50  
51  
52  
53  
54 172 Eq. 1 
$$\text{EF} = \frac{I_{\text{SERS}}/c_{\text{SERS}}}{I_{\text{RS}}/c_{\text{RS}}} = \frac{I_{\text{SERS}}}{I_{\text{RS}}}$$

1  
2  
3 173 Since sample preparation for SERS and non-SERS conditions was identical, the concentration  
4  
5 174  $c_{\text{SERS}}$  can be assumed to be equal to  $c_{\text{RS}}$  and the equation to calculate EFs can be simplified to a  
6  
7  
8 175 comparison of  $I_{\text{SERS}}$  and  $I_{\text{RC}}$ .  $I_{\text{SERS}}$  and  $I_{\text{RC}}$  are represented by the integrated peak area for the  
9  
10 176 respective vibrational modes. Integrated peak areas were determined along the natural baseline  
11  
12 177 of the spectra using a multipeak fitting software package (Igor Pro, WaveMetrics). The average  
13  
14 178 integrated peak area for Raman spectra collected under non-SERS conditions was used for  $I_{\text{RC}}$ .

### 179 3 Results and Discussion

180 Laboratory-generated aerosol particle standards were used to investigate enhancement  
181 from various Ag SERS substrates, including AgNP coated quartz and Ag foil, and their  
182 application to aerosol particle studies, specifically particles  $<1 \mu\text{m}$ . Raman spectra of standard  
183 PSL particles sized 400 nm, 600 nm, and 800 nm collected from each substrate showed that,

184 while both Ag SERS substrates  
185 enhanced the Raman signal across  
186 all vibrational modes, Ag foil  
187 yielded significantly higher EFs  
188 (Figure 1). Raman spectra were  
189 successfully collected for PSL

190 particles of all sizes on the Ag foil  
191 and quartz substrates, but due to low  
192 intensity and the resulting small  
193 enhancement, only the 800 nm PSLs  
194 were tested with the AgNP  
195 substrate. Even though Raman

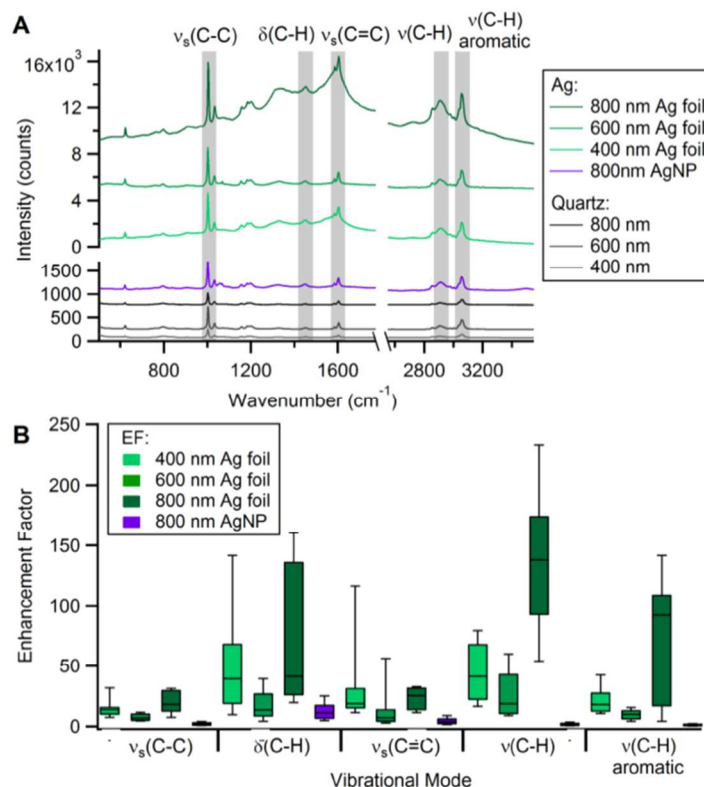


**Figure 1.** (A) Average Raman spectra for 400 nm, 600 nm, and 800 nm PSL particles on quartz, Ag foil, and AgNP substrates. (B) Box and whisker plot of calculated EFs for vibrational modes of interest for all particle sizes. The center line represents the median, the box outlines the inner quartiles, and the whiskers represent the 10<sup>th</sup> and 90<sup>th</sup> percentile.

1  
2  
3 196 signal was detected for PSL particles on plain quartz substrate, intensity was very low and  
4  
5 197 vibrational modes were difficult to distinguish from background noise, particularly for the 400  
6  
7  
8 198 nm sized particles. For the 800 nm PSL particles, EFs for the symmetric ring stretching modes,  
9  
10 199  $\nu_s(\text{C-C})^{98-100}$  at  $1000\text{ cm}^{-1}$  and  $\nu_s(\text{C=C})^{98-100}$  at  $1602\text{ cm}^{-1}$ , ranged for 7 to 32 and 11 to 33,  
11  
12 200 respectively, for the Ag foil and 1 to 4 and 2 to 9 for the AgNP substrate, respectively. In  
13  
14  
15 201 comparison to the ring stretching modes, C-H bending and stretching modes showed greater  
16  
17 202 enhancement in response to the SERS effect. EFs for the C-H bending mode ( $\delta(\text{C-H})$ ,  $1452\text{ cm}^{-1}$ ),  
18  
19 203  $\nu_s(\text{C-C})^{98,99}$ , C-H stretching mode ( $\nu(\text{C-H})$ ,  $2908\text{ cm}^{-1}$ ),<sup>98,99</sup> and aromatic C-H stretching mode ( $\nu(\text{C-H})$   
20  
21 204 aromatic,  $3054\text{ cm}^{-1}$ )<sup>98,99</sup> ranged from 20 to 161, 54 to 233, and 4 to 142, respectively, for the Ag  
22  
23  
24 205 foil and 5 to 26, 1 to 4, and 1 to 3, respectively, for the AgNP substrate. The EF values for the  
25  
26 206 AgNP substrate samples are consistent with previously reported EF values for  $(\text{NH}_4)_2\text{SO}_4$  and  
27  
28 207  $\text{NaNO}_3$  standard particles analyzed with SERS using similar substrates.<sup>87</sup> SERS enhancement  
29  
30 208 was observed for the 400 and 600 nm sized particles on Ag foil and EFs for the five PSL  
31  
32  
33 209 vibrational modes ranged from 4 to 151, with the  $\delta(\text{C-H})$  and  $\nu(\text{C-H})$  modes again exhibiting the  
34  
35  
36 210 largest enhancements. All Raman spectra, for PSL particles on both quartz and Ag foil, are  
37  
38 211 provided in the Supplementary Information. It should be noted that both the 400 nm and 600 nm  
39  
40 212 particles are smaller than the 721 nm diameter of the laser spot (for a 532 nm laser with 0.9 N.A.  
41  
42 213 objective).

43  
44  
45 214 The large variability in EFs, particularly evident for the Ag foil samples, could be  
46  
47 215 attributed to varying degrees of coupling between LSPRs with analytes depending on location of  
48  
49 216 the particle with respect to the SERS-enhanced volume on the rough surface of the Ag foil or  
50  
51 217 inconsistent distribution of AgNPs. Preliminary work testing several other Ag SERS substrates is  
52  
53 218 included in the Supplementary Information and results were, at best, comparable to the AgNP  
54  
55  
56  
57  
58  
59  
60

1  
2  
3 219 enhancement shown here. Despite the variability in enhancement, the Ag foil substrate yielded  
4  
5 220 the highest EFs and thus, was used as the SERS substrate for all subsequent experiments in this  
6  
7  
8 221 work.

9  
10 222 Across all vibrational modes, there was no clear relationship between particle size and  
11  
12 223 enhancement. Enhancement was expected to increase with increasing particle size, as the higher  
13  
14 224 number of analyte molecules present in the larger particles could enable more opportunities for  
15  
16  
17 225 coupling to LSPRs and lead to greater enhancement of the Raman signal. This was observed  
18  
19 226 somewhat for the largest and smallest sized PSL particles analyzed, as the 800 nm particles were  
20  
21 227 consistently more enhanced than the 400 nm particles, but the 600 nm particles exhibited the  
22  
23  
24 228 lowest levels of enhancement. The cause for the low enhancement observed for the 600 nm PSL  
25  
26 229 particles is unclear at this time, but could possibly be due to PSL quality, crowding effects, or the  
27  
28 230 arrangement of PSL molecules hindering coupling between LSPRs and analyte molecules. The  
29  
30  
31 231 cause of the low enhancement for the 600 nm PSL particles remains unclear, as the inorganic  
32  
33 232 particles investigated as part of this study (discussed below) were more consistent with the 400  
34  
35 233 nm and 800 nm PSL particles, with larger sized particles yielding more enhanced spectra.

36  
37 234 In addition to PSL particles, which are primarily organic,  $(\text{NH}_4)_2\text{SO}_4$  and  $\text{NaNO}_3$   
38  
39 235 particles were also tested since atmospheric aerosol particles often contain these inorganic  
40  
41  
42 236 components.<sup>101</sup>  $(\text{NH}_4)_2\text{SO}_4$  and  $\text{NaNO}_3$  particles were generated from solution and size-selected  
43  
44 237 at 400 nm, 600 nm, and 800 nm for SERS analysis. For  $(\text{NH}_4)_2\text{SO}_4$ , the  $\nu(\text{SO}_4^{2-})$  and the  $\nu(\text{N-H})$   
45  
46  
47 238 stretching mode of  $\text{NH}_4^+$  were studied (Figure 2). The  $\nu_1(\text{SO}_4^{2-})$ <sup>44,46,47,102,103</sup> mode at  $963\text{ cm}^{-1}$   
48  
49 239 had EFs ranging from 30 to 841, which is up to ~420 times greater than the average EFs  
50  
51 240 reported by Craig et al. using AgNP SERS substrates.<sup>87</sup> There was a red shift in peak location for  
52  
53  
54 241 the SERS enhanced  $\nu_1(\text{SO}_4^{2-})$  mode, shifting from  $975\text{ cm}^{-1}$  to  $963\text{ cm}^{-1}$ , along with an increase

242 in peak broadness. This shift is possibly  
 243 attributed to charge-transfer interactions  
 244 between Ag and the  $(\text{NH}_4)_2\text{SO}_4$  molecules  
 245 and is consistent with earlier work studying  
 246 SERS enhancement of  $(\text{NH}_4)_2\text{SO}_4$ /sucrose  
 247 particles.<sup>90</sup> The  $\nu(\text{N-H})$ <sup>102,103</sup> mode centered  
 248 at  $3130\text{ cm}^{-1}$  had EFs ranging from 33 to  
 249 730. It should be noted that  $\nu(\text{N-H})$  is  
 250 broader due to hydrogen bonding and can  
 251 be difficult to quantify in low-intensity  
 252 spectra. For  $\text{NaNO}_3$ , three stretches  
 253 corresponding to  $\text{NO}_3^-$  were studied (Figure  
 254 3).  $\nu_1(\text{NO}_3^-)$ <sup>47,103,104</sup> at  $1067\text{ cm}^{-1}$  had EFs  
 255 ranging from 8 to 48, which is up to ~16  
 256 times greater than the average EFs reported  
 257 by Craig et al. using AgNP SERS

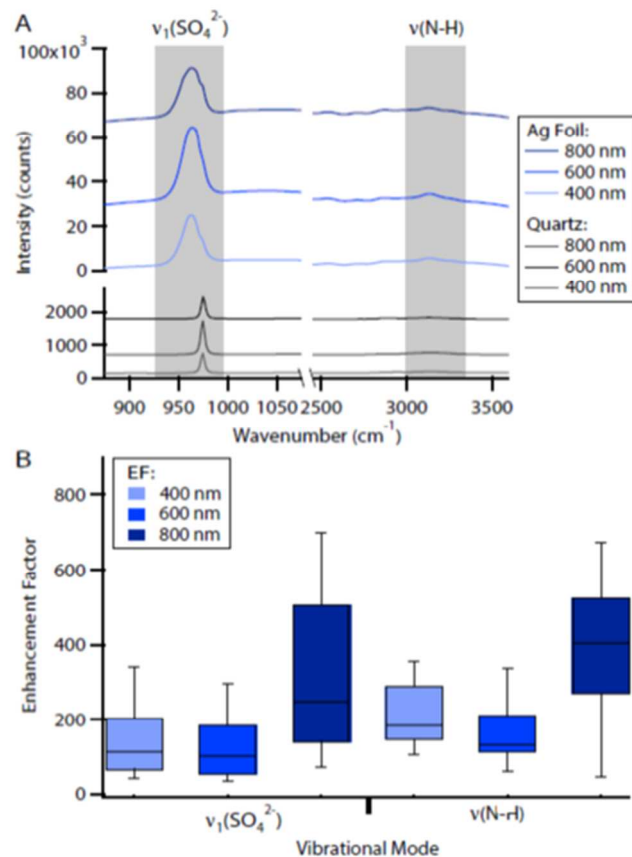


**Figure 2.** (A) Average Raman spectra for 400 nm, 600 nm, and 800 nm  $(\text{NH}_4)_2\text{SO}_4$  particles on quartz and Ag foil substrates. (B) Box and whisker plot of calculated EFs for vibrational modes of interest for all particle sizes. The center line represents the median, the box outlines the inner quartiles, and the whiskers represent the 10<sup>th</sup> and 90<sup>th</sup> percentile.

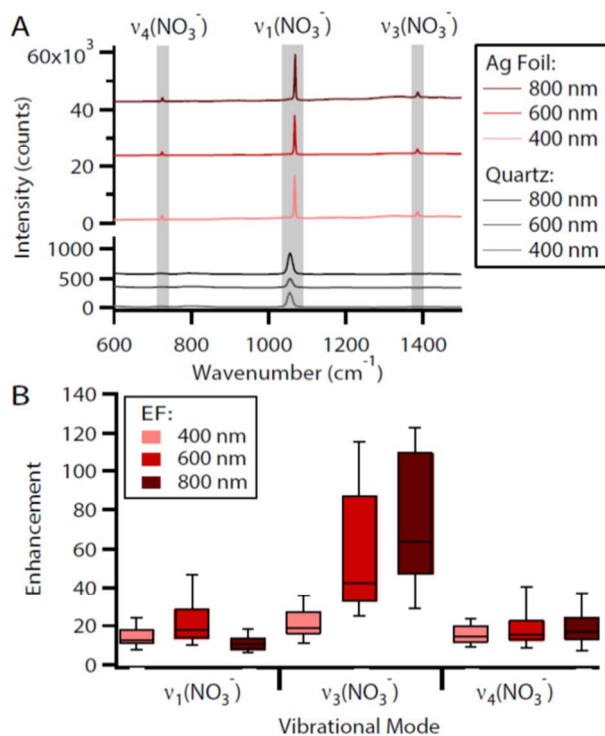


**Figure 3.** (A) Average Raman spectra for 400 nm, 600 nm, and 800 nm  $\text{NaNO}_3$  particles on quartz and Ag foil substrates. (B) Box and whisker plot of calculated EFs for vibrational modes of interest for all particle sizes. The center line represents the median, the box outlines the inner quartiles, and the whiskers represent the 10<sup>th</sup> and 90<sup>th</sup> percentile.

substrates.<sup>87</sup> There was a slight blue shift in peak location for the SERS enhanced  $\nu_1(\text{NO}_3^-)$  mode, shifting from  $1056 \text{ cm}^{-1}$  to  $1067 \text{ cm}^{-1}$ , along with an increase in peak sharpness. The  $1054 \text{ cm}^{-1}$  mode corresponds to aqueous, free  $\text{NO}_3^-$ , while the  $1067 \text{ cm}^{-1}$  mode corresponds to  $\text{Na}^+$ -bound  $\text{NO}_3^-$ .<sup>69,103</sup> Interestingly, this result is inconsistent with previous work that observed a red shift from  $1067 \text{ cm}^{-1}$  to  $1054 \text{ cm}^{-1}$  for  $\nu_1(\text{NO}_3^-)$ .<sup>87,105</sup> Previous work

proposed that  $\text{NaNO}_3$  cannot couple as effectively as  $\text{NO}_3^-$  with the Ag substrate due to interaction with sodium or incorporation into a  $\text{NaNO}_3$  amorphous solid or crystal, leading to a red shift occurring with increased

272

enhancement.<sup>87</sup> Experimental conditions, such as RH impacts on particle phase, could play a role,

274 but further work is needed to characterize this phenomenon and reconcile the discrepancy in

275 observed peak shifting. Other modes,  $\nu_3(\text{NO}_3^-)$ <sup>103,104</sup> at  $1386 \text{ cm}^{-1}$  and  $\nu_4(\text{NO}_3^-)$ <sup>103,104</sup> at  $725 \text{ cm}^{-1}$ ,

276 had larger EFs, ranging from 5 to 116, and no observable peak shifts. All Raman spectra, for

277  $(\text{NH}_4)_2\text{SO}_4$  and  $\text{NaNO}_3$  particles on both quartz and Ag foil, are provided in the Supplementary

278 Information.

279 Qualitative observation shows that EFs increased with increasing particle size for the

280 vibrational modes studied for the 400 nm and 800 nm  $(\text{NH}_4)_2\text{SO}_4$  particles. As discussed

1  
2  
3 281 previously, this could be attributed to the higher number of analyte molecules present in the  
4  
5 282 larger particles and the greater probability that a portion of the particle would be within the  
6  
7  
8 283 enhanced region of a LSPR after impaction leading to greater observed enhancement. An  
9  
10 284 alternate explanation for increased enhancement is the accumulation of crystals or ions at the foil  
11  
12 285 interface as aqueous particles spread upon impaction. This effect applies only to the  $(\text{NH}_4)_2\text{SO}_4$   
13  
14 286 and  $\text{NaNO}_3$  particles, as the PSL particles are solid. Similar to the PSL particles, the 600 nm  
15  
16  
17 287  $(\text{NH}_4)_2\text{SO}_4$  particles exhibited the lowest enhancement. There is no apparent trend for the EFs for  
18  
19 288 the vibrational modes studied for all sized  $\text{NaNO}_3$  particles. Also, as with the PSL particles, there  
20  
21 289 was a high level of variability in enhancement for all of the  $(\text{NH}_4)_2\text{SO}_4$  and  $\text{NaNO}_3$  vibrational  
22  
23  
24 290 modes. Further testing with more samples, both in terms of particle sizes studied and number of  
25  
26 291 particles analyzed, is necessary to resolve any trends or relationships between particle size and  
27  
28 292 enhancement.

29  
30  
31 293 Thus far in this study, through SERS, the smallest particle size shown has been 400 nm,  
32  
33 294 which is about 2-3 times smaller than the size of aerosol particles typically characterized through  
34  
35 295 Raman analysis. However, SERS is capable of single molecule detection and so, should allow  
36  
37  
38 296 for Raman analysis of aerosol particles < 400 nm. To test this limit, 150 nm PSL particles were  
39  
40 297 collected on Ag foil. It should be noted that a 150 nm sized particle is well below to the  
41  
42 298 diffraction limit of visible light and the Raman spectrometer used in this study (300-400 nm and  
43  
44 299 361 nm, respectively), making individual particle identification challenging. Automated point-  
45  
46  
47 300 by-point mapping with a step size of 0.25  $\mu\text{m}$  was used over a larger region of the substrate,  
48  
49 301 enabling spectra to be collected for the 150 nm particles that were difficult to distinguish  
50  
51 302 optically due to spatial resolution limitations. A representative spectrum for a 150 nm PSL  
52  
53  
54 303 particle and its corresponding location are shown in Figure 4. The five vibrational modes focused



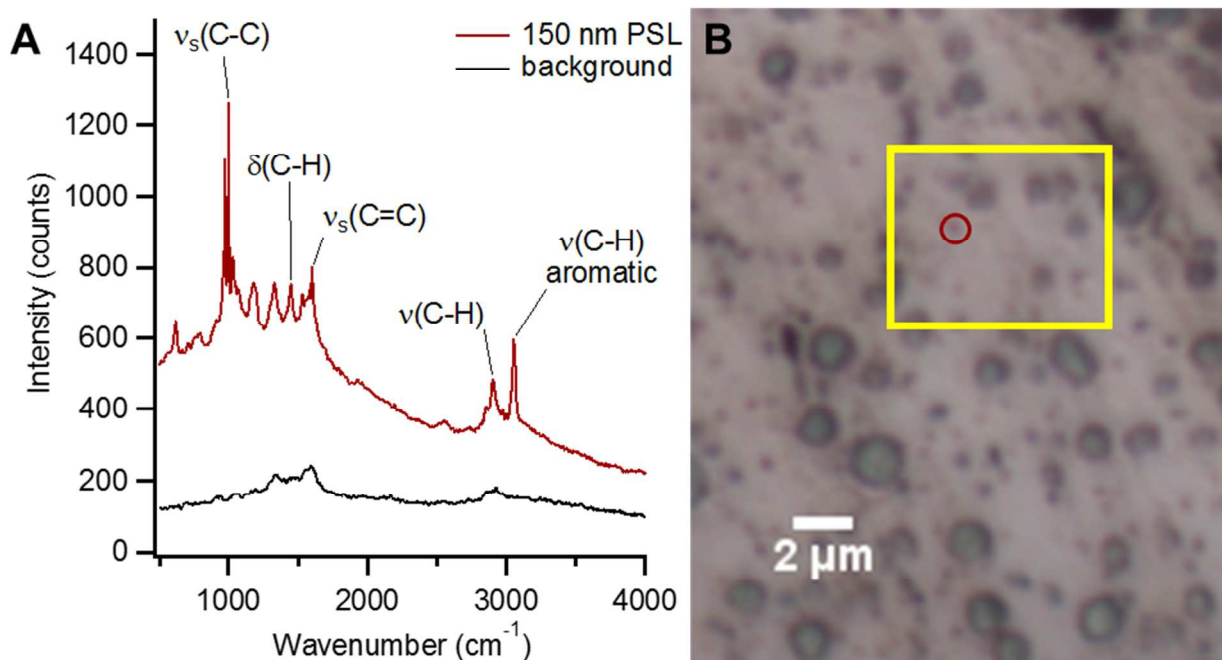


**Figure 4.** (A) SERS spectrum collected via automated point-by-point mapping of a 150 nm PSL particle on Ag foil substrate. (B) Optical image of 150 nm PSL sample on Ag foil, with the yellow box highlighting the mapped area and the red circle indicating the location of the Raman spectrum shown in (A).

on in the earlier analysis are indicated, though other vibrational modes were also enhanced and present. In the optical image, the yellow box highlights the mapped region, while the red circle indicates the point corresponding to the SERS PSL spectrum. The small, dark spots are individual 150 nm PSL particles, while the larger spots are most likely agglomerates and were avoided for this analysis. It should also be noted that marks and scratches to the Ag foil can lead to intensity in the Raman spectra that make it difficult to identify vibrational modes corresponding to the particles. To reduce substrate interference, smooth regions of the Ag foil were selected for mapping analysis.

In addition to testing SERS with laboratory-generated aerosol standards below the diffraction limit, ambient aerosol particles were also sampled, size-selected at 150 nm, and impacted in a same manner (Figure 5). Based on the sampling time and aerosol concentrations, the substrate has primarily individual particles with minimal overlap. While it is difficult to

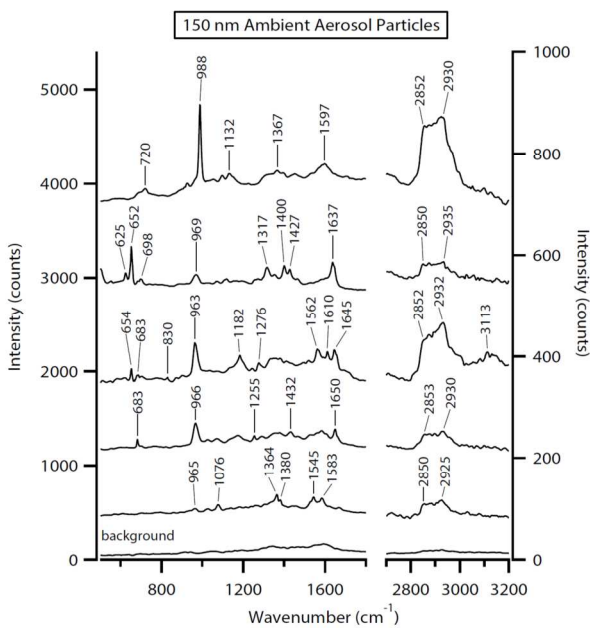


**Figure 5.** SERS-enhanced spectra obtained from Raman mapping of 150 nm size-selected ambient aerosol particles.

316 definitively identify vibrational modes in  
 317 ambient aerosol due to their complex  
 318 chemical composition and overlapping  
 319 regions where modes can be present, tentative  
 320 assignments are proposed. Peaks in the 500-  
 321 900  $\text{cm}^{-1}$  region could correspond to  $\nu(\text{Si-O-Si})$ ,  $\delta(\text{Si-O-Al})$ , and other lattice vibrations of  
 322 fly ash or silicon and aluminosilicate  
 323 minerals,<sup>54,98,106-108</sup>  $\delta(\text{C-O})$  of carbonates and  
 324 carboxylic acids,<sup>54,87,98</sup> or “breathing” modes  
 325 of aromatic rings.<sup>57</sup> The peaks at 963 – 988

327  $\text{cm}^{-1}$  most likely correspond to  $\nu_1(\text{SO}_4^{2-})$ ,<sup>44,46,47,102,103</sup> and are exhibiting the same red shift  
 328 observed for the  $(\text{NH}_4)_2\text{SO}_4$  standard particles discussed earlier.<sup>90</sup> Peaks in the 1000-1700  $\text{cm}^{-1}$   
 329 region could correspond to a range of vibrational modes of organic functional groups, including  
 330 stretching modes, such as  $\nu(\text{C-O})$ ,  $\nu(\text{C-C})$ ,  $\nu(\text{C=C})$ ,  $\nu(\text{COO}^-)$ , and  $\nu(\text{C-OH})$ , and bending and  
 331 twisting modes, such as  $\delta(\text{CH}_2)$ ,  $\delta(\text{CH}_3)$ ,  $\delta(\text{C-C})$ ,  $\delta(\text{O-C-O})$ , and  $\delta(\text{O-H})$ .<sup>44,47,54,57-60,67,98,109,110</sup>  
 332 Peaks in the higher energy 2700-3000  $\text{cm}^{-1}$  region correspond to symmetric and asymmetric  
 333  $\nu(\text{CH}_2)$  and  $\nu(\text{CH}_3)$  modes.<sup>44,47,54,57,59,98</sup> Specific compounds present in the ambient aerosol  
 334 particles related to these functional groups could include long chain aliphatics, glyoxal  
 335 oligomers, peroxides, organic sulfates, and minerals associated with dust.<sup>47,54,59,60,70</sup> To our  
 336 knowledge, this is the first SERS-enhanced spectroscopic analysis of aerosol particles that have a  
 337 smaller diameter than the visible light diffraction limit, an important step towards measurements  
 338 of aerosol particles in a key size range for atmospheric surface chemistry. Additionally, for these

1  
2  
3 339 ambient spectra, vibrational modes attributed to organic species exhibited greater enhancement  
4  
5 340 in the lower frequency region (1000 – 1800  $\text{cm}^{-1}$ ) than the higher frequency region (2700 – 3000  
6  
7 341  $\text{cm}^{-1}$ ), which is consistent with previous work with SERS of ambient particles.<sup>87</sup> This  
8  
9  
10 342 demonstrates the potential for SERS to enable the study of vibrational modes that are not as well  
11  
12 343 characterized in the literature due to the difficulties associated with detecting them in aerosol  
13  
14 344 particles via traditional microspectroscopic methods.

15  
16  
17 345  
18 346 **4 Conclusions**

19  
20 347 SERS was applied to the study of atmospheric aerosol particles to improve the limit of  
21  
22 348 detection in terms of particles size. 400 nm, 600 nm, and 800 nm size-selected laboratory-  
23  
24 349 generated aerosol particle standards of PSLs, ammonium sulfate, and sodium nitrate were  
25  
26  
27 350 collected on Ag foil SERS substrates and analyzed. Average enhancement factors for a range of  
28  
29 351 inorganic and organic vibrational modes were calculated to be on the order of  $10^2$  and as large as  
30  
31 352 530. SERS enhancements may increase with increasing particle size, as observed with the 400  
32  
33 353 nm and 800 nm PSL and  $(\text{NH}_4)_2\text{SO}_4$  standards, but the 600 nm PSL and  $(\text{NH}_4)_2\text{SO}_4$  had the  
34  
35  
36 354 lowest EF values and there was no observed consistent trend between SERS enhancement and  
37  
38 355 particle size for the  $\text{NaNO}_3$  standard. These results are likely due to variability in LSPRs on the  
39  
40 356 foil surface and subsequent coupling with analyte molecules. Further testing with more particle  
41  
42  
43 357 sizes and increased number of particles analyzed is necessary to resolve a definitive relationship  
44  
45 358 between particle size and enhancement. Ag foil substrates were also used for SERS analysis of  
46  
47 359 150 nm PSL and ambient aerosol particles via automated Raman mapping. All five PSL  
48  
49 360 vibrational modes characterized with the larger sized particles were identified in the SERS  
50  
51 361 enhanced spectra of the 150 nm particles. For the ambient aerosol, a range of inorganic and  
52  
53  
54 362 organic vibrational modes were detected, and corresponding functional groups were proposed.

1  
2  
3 363 To our knowledge, this is the first vibrational spectroscopic analysis of aerosol particles  
4  
5 364 approaching the mode of the atmospheric number size distribution (~100 nm). These results  
6  
7  
8 365 show the potential for SERS to enable improved analysis of aerosol particle chemical  
9  
10 366 composition and mixing state for the most atmospherically abundant particle sizes. The ability to  
11  
12 367 detect chemical species in these small volume particles also shows the potential for future SERS  
13  
14 368 work to probe differences in composition at aerosol surfaces due to phase separation, the  
15  
16  
17 369 presence of surfactants, or surface-level reactions. Overall, future SERS studies of atmospheric  
18  
19 370 aerosol composition could lead to improved understanding of multiphase atmospheric processing  
20  
21  
22 371 and aerosol impacts on climate and human health.

23  
24 372

### 25 26 373 **Conflicts of Interest**

27  
28 374 There are no conflicts to declare.

29  
30  
31 375

### 32 33 376 **Acknowledgments**

34  
35 377 This work was supported by the National Science Foundation Grant No. CAREER-1654149 and  
36  
37 378 startup funds from the University of Michigan. RLC was partially supported by the Susan  
38  
39  
40 379 Lipschutz Fellowship Award from the University of Michigan Rackham Graduate School. DBT  
41  
42 380 was partially supported by the Detroit Research Internship Summer Experience (D-  
43  
44 381 RISE) program, funded by the NSF (CHE-1305777) to Dr. Nicolai Lehnert at UM, the UM  
45  
46  
47 382 College of Literature, Science and the Arts, the UM Office of the Provost, and Cass Technical  
48  
49 383 High School in Detroit, MI. The Pratt Lab at the University of Michigan is acknowledged for  
50  
51 384 assistance with ambient aerosol sampling.

52  
53  
54 385

386 **References**

- 387 1 L. Di Girolamo, T. C. Bond, D. Bramer, D. J. Diner, F. Fettinger, R. A. Kahn, J. V  
388 Martonchik, M. V Ramana, V. Ramanathan and P. J. Rasch, Analysis of Multi-angle  
389 Imaging SpectroRadiometer (MISR) aerosol optical depths over greater India during  
390 winter 2001-2004, *Geophys. Res. Lett.*, 2004, **31**, L23115, DOI: 10.1029/2004GL021273.
- 391 2 U. Pöschl, Atmospheric aerosols: Composition, transformation, climate and health effects,  
392 *Angew. Chemie-International Ed.*, 2005, **44**, 7520–7540.
- 393 3 M. O. Andreae and D. Rosenfeld, Aerosol-cloud-precipitation interactions. Part 1. The nature  
394 and sources of cloud-active aerosols, *Earth-Science Rev.*, 2008, **89**, 13–41.
- 395 4 P. J. DeMott, T. C. J. Hill, C. S. McCluskey, K. A. Prather, D. B. Collins, R. C. Sullivan, M.  
396 J. Ruppel, R. H. Mason, V. E. Irish, T. Lee, C. Y. Hwang, T. S. Rhee, J. R. Snider, G. R.  
397 McMeeking, S. Dhaniyala, E. R. Lewis, J. J. B. Wentzell, J. Abbatt, C. Lee, C. M.  
398 Sultana, A. P. Ault, J. L. Axson, M. Diaz Martinez, I. Venero, G. Santos-Figueroa, M. D.  
399 Stokes, G. B. Deane, O. L. Mayol-Bracero, V. H. Grassian, T. H. Bertram, A. K.  
400 Bertram, B. F. Moffett and G. D. Franc, Sea spray aerosol as a unique source of ice  
401 nucleating particles, *Proc. Natl. Acad. Sci.*, 2016, **113**, 5797–5803.
- 402 5 A. P. Ault, C. R. Williams, A. B. White, P. J. Neiman, J. M. Creamean, C. J. Gaston, F. M.  
403 Ralph and K. A. Prather, Detection of Asian dust in California orographic precipitation,  
404 *J. Geophys. Res.*, 2011, **116**, D16205.
- 405 6 J. M. Creamean, K. J. Suski, D. Rosenfeld, A. Cazorla, P. J. DeMott, R. C. Sullivan, A. B.  
406 White, F. M. Ralph, P. Minnis, J. M. Comstock, J. M. Tomlinson and K. A. Prather, Dust  
407 and biological aerosols from the Sahara and Asia influence precipitation in the western  
408 U.S, *Science.*, 2013, **339**, 1572–1578.
- 409 7 J. M. Creamean, A. P. Ault, A. B. White, P. J. Neiman, F. M. Ralph, P. Minnis and K. A.  
410 Prather, Impact of interannual variations in sources of insoluble aerosol species on  
411 orographic precipitation over California’s central Sierra Nevada, *Atmos. Chem. Phys.*,  
412 2015, **15**, 6535–6548.
- 413 8 K. A. Prather, C. D. Hatch and V. H. Grassian, Analysis of Atmospheric Aerosols, *Annu.*  
414 *Rev. Anal. Chem.*, 2008, **1**, 485–514.
- 415 9 A. P. Ault and J. L. Axson, Atmospheric Aerosol Chemistry: Spectroscopic and Microscopic  
416 Advances, *Anal. Chem.*, 2017, **89**, 430–452.
- 417 10 K. A. Prather, T. H. Bertram, V. H. Grassian, G. B. Deane, M. D. Stokes, P. J. DeMott, L. I.  
418 Aluwihare, B. P. Palenik, F. Azam, J. H. Seinfeld, R. C. Moffet, M. J. Molina, C. D.  
419 Cappa, F. M. Geiger, G. C. Roberts, L. M. Russell, A. P. Ault, J. Baltrusaitis, D. B.  
420 Collins, C. E. Corrigan, L. A. Cuadra-Rodriguez, C. J. Ebben, S. D. Forestieri, T. L.  
421 Guasco, S. P. Hersey, M. J. Kim, W. F. Lambert, R. L. Modini, W. Mui, B. E. Pedler, M.  
422 J. Ruppel, O. S. Ryder, N. G. Schoepp, R. C. Sullivan and D. Zhao, Bringing the ocean  
423 into the laboratory to probe the chemical complexity of sea spray aerosol, *Proc. Natl.*  
424 *Acad. Sci.*, 2013, **110**, 7550–7555.
- 425 11 N. Riemer and M. West, Quantifying aerosol mixing state with entropy and diversity  
426 measures, *Atmos. Chem. Phys.*, 2013, **13**, 11423–11439.
- 427 12 O. S. Ryder, A. P. Ault, J. F. Cahill, T. L. Guasco, T. P. Riedel, L. A. Cuadra-Rodriguez, C.  
428 J. Gaston, E. Fitzgerald, C. Lee, K. A. Prather and T. H. Bertram, On the Role of Particle  
429 Inorganic Mixing State in the Reactive Uptake of N<sub>2</sub>O<sub>5</sub> to Ambient Aerosol Particles,  
430 *Environ. Sci. Technol.*, 2014, **48**, 1618–1627.
- 431 13 E. Fitzgerald, A. P. Ault, M. D. Zauscher, O. L. Mayol-Bracero and K. A. Prather,

- 1  
2  
3 432 Comparison of the mixing state of long-range transported Asian and African mineral  
4 433 dust, *Atmos. Environ.*, 2015, **115**, 19–25.
- 5 434 14 A. P. Ault, C. J. Gaston, Y. Wang, G. Dominguez, M. H. Thiemens and K. A. Prather,  
6 435 Characterization of the Single Particle Mixing State of Individual Ship Plume Events  
7 436 Measured at the Port of Los Angeles, *Environ. Sci. Technol.*, 2010, **44**, 1954–1961.
- 8 437 15 R. M. Healy, N. Riemer, J. C. Wenger, M. Murphy, M. West, L. Poulain, A. Wiedensohler, I.  
9 438 P. O'Connor, E. McGillicuddy, J. R. Sodeau and G. J. Evans, Single particle diversity  
10 439 and mixing state measurements, *Atmos. Chem. Phys.*, 2014, **14**, 6289–6299.
- 11 440 16 R. E. O'Brien, B. B. Wang, A. Laskin, N. Riemer, M. West, Q. Zhang, Y. L. Sun, X. Y. Yu,  
12 441 P. Alpert, D. A. Knopf, M. K. Gilles and R. C. Moffet, Chemical imaging of ambient  
13 442 aerosol particles: Observational constraints on mixing state parameterization, *J. Geophys.*  
14 443 *Res.*, 2015, **120**, 9591–9605.
- 15 444 17 L. Fierce, T. C. Bond, S. E. Bauer, F. Mena and N. Riemer, Black carbon absorption at the  
16 445 global scale is affected by particle-scale diversity in composition, 2016, **7**, 12361.
- 17 446 18 D. B. Collins, A. P. Ault, R. C. Moffet, M. J. Ruppel, L. A. Cuadra-Rodriguez, T. L. Guasco,  
18 447 C. E. Corrigan, B. E. Pedler, F. Azam, L. I. Aluwihare, T. H. Bertram, G. C. Roberts, V.  
19 448 H. Grassian and K. A. Prather, Impact of marine biogeochemistry on the chemical mixing  
20 449 state and cloud forming ability of nascent sea spray aerosol, *J. Geophys. Res.*, 2013, **118**,  
21 450 8553–8565.
- 22 451 19 A. P. Ault, R. C. Moffet, J. Baltrusaitis, D. B. Collins, M. J. Ruppel, L. A. Cuadra-  
23 452 Rodriguez, D. Zhao, T. L. Guasco, C. J. Ebben, F. M. Geiger, T. H. Bertram, K. A.  
24 453 Prather and V. H. Grassian, Size-dependent changes in sea spray aerosol composition and  
25 454 properties with different seawater conditions, *Environ. Sci. Technol.*, 2013, **47**, 5603–  
26 455 5612.
- 27 456 20 M. Hallquist, J. C. Wenger, U. Baltensperger, Y. Rudich, D. Simpson, M. Claeys, J.  
28 457 Dommen, N. M. Donahue, C. George, A. H. Goldstein, J. F. Hamilton, H. Herrmann, T.  
29 458 Hoffmann, Y. Iinuma, M. Jang, M. E. Jenkin, J. L. Jimenez, A. Kiendler-Scharr, W.  
30 459 Maenhaut, G. McFiggans, T. F. Mentel, A. Monod, A. S. H. Prevot, J. H. Seinfeld, J. D.  
31 460 Surratt, R. Szmigielski and J. Wildt, The formation, properties and impact of secondary  
32 461 organic aerosol: current and emerging issues, *Atmos. Chem. Phys.*, 2009, **9**, 5155–5236.
- 33 462 21 P. J. Ziemann and R. Atkinson, Kinetics, products, and mechanisms of secondary organic  
34 463 aerosol formation, *Chem. Soc. Rev.*, 2012, **41**, 6582–6605.
- 35 464 22 V. F. McNeill, Aqueous organic chemistry in the atmosphere: Sources and chemical  
36 465 processing of organic aerosols, *Environ. Sci. Technol.*, 2015, **49**, 1237–1244.
- 37 466 23 A. Virtanen, J. Joutsensaari, T. Koop, J. Kannosto, P. Yli-Pirila, J. Leskinen, J. M. Makela, J.  
38 467 K. Holopainen, U. Poeschl, M. Kulmala, D. R. Worsnop and A. Laaksonen, An  
39 468 amorphous solid state of biogenic secondary organic aerosol particles, *Nature*, 2010, **467**,  
40 469 824–827.
- 41 470 24 Y. You, M. L. Smith, M. Song, S. T. Martin and A. K. Bertram, Liquid–liquid phase  
42 471 separation in atmospherically relevant particles consisting of organic species and  
43 472 inorganic salts, *Int. Rev. Phys. Chem.*, 2014, **33**, 43–77.
- 44 473 25 B. Wang, R. E. O'Brien, S. T. Kelly, J. E. Shilling, R. C. Moffet, M. K. Gilles and A. Laskin,  
45 474 Reactivity of liquid and semisolid secondary organic carbon with chloride and nitrate in  
46 475 atmospheric aerosols, *J. Phys. Chem. A*, 2015, **119**, 4498–4508.
- 47 476 26 M. L. Smith, Y. You, M. Kuwata, A. K. Bertram and S. T. Martin, Phase transitions and  
48 477 phase miscibility of mixed particles of ammonium sulfate, toluene-derived secondary

- 1  
2  
3 478 organic material, and water, *J. Phys. Chem. A*, 2013, **117**, 8895–8906.
- 4 479 27 A. P. Ault, T. L. Guasco, O. S. Ryder, J. Baltrusaitis, L. A. Cuadra-Rodriguez, D. B. Collins,  
5 480 M. J. Ruppel, T. H. Bertram, K. A. Prather and V. H. Grassian, Inside versus outside: Ion  
6 481 redistribution in nitric acid reacted sea spray aerosol particles as determined by single  
7 482 particle analysis, *J. Am. Chem. Soc.*, 2013, **135**, 14528–14531.
- 8 483 28 D. J. Losey, R. G. Parker and M. A. Freedman, pH dependence of liquid–liquid phase  
9 484 separation in organic aerosol, *J. Phys. Chem. Lett.*, 2016, **7**, 3861–3865.
- 10 485 29 C. J. Ebben, A. P. Ault, M. J. Ruppel, O. S. Ryder, T. H. Bertram, V. H. Grassian, K. A.  
11 486 Prather and F. M. Geiger, Size-resolved sea spray aerosol particles studied by vibrational  
12 487 sum frequency generation, *J. Phys. Chem. A*, 2013, **117**, 6589–6601.
- 13 488 30 J. F. Davies and K. R. Wilson, Nanoscale interfacial gradients formed by the reactive uptake  
14 489 of OH radicals onto viscous aerosol surfaces, *Chem. Sci.*, 2015, **6**, 7020–7027.
- 15 490 31 S. Sobanska, J. Barbillat, M. Moreau, N. Nuns, I. De Waele, D. Petitprez, Y. Tobon and C.  
16 491 Bremard, Influence of stearic acid coating of the NaCl surface on the reactivity with NO<sub>2</sub>  
17 492 under humidity, *Phys. Chem. Chem. Phys.*, 2015, **17**, 10963–10977.
- 18 493 32 J. D. Raff, B. Njegic, W. L. Chang, M. S. Gordon, D. Dabdub, R. B. Gerber and B. J.  
19 494 Finlayson-Pitts, Chlorine activation indoors and outdoors via surface-mediated reactions  
20 495 of nitrogen oxides with hydrogen chloride, *Proc. Natl. Acad. Sci. U. S. A.*, 2009, **106**,  
21 496 13647–13654.
- 22 497 33 G. Rubasinghege, S. Elzey, J. Baltrusaitis, P. M. Jayaweera and V. H. Grassian, Reactions on  
23 498 atmospheric dust particles: Surface photochemistry and size-dependent nanoscale redox  
24 499 chemistry, *J. Phys. Chem. Lett.*, 2010, **1**, 1729–1737.
- 25 500 34 G. Rubasinghege and V. H. Grassian, Role(s) of adsorbed water in the surface chemistry of  
26 501 environmental interfaces, *Chem. Commun.*, 2013, **49**, 3071–3094.
- 27 502 35 C. D. Hatch, K. M. Gierlus, J. D. Schuttlefield and V. H. Grassian, Water adsorption and  
28 503 cloud condensation nuclei activity of calcite and calcite coated with model humic and  
29 504 fulvic acids, *Atmos. Environ.*, 2008, **42**, 5672–5684.
- 30 505 36 L. Renbaum-Wolff, J. W. Grayson, A. P. Bateman, M. Kuwata, M. Sellier, B. J. Murray, J.  
31 506 E. Shilling, S. T. Martin and A. K. Bertram, Viscosity of  $\alpha$ -pinene secondary organic  
32 507 material and implications for particle growth and reactivity, *Proc. Natl. Acad. Sci.*, 2013,  
33 508 **110**, 8014–8019.
- 34 509 37 J. P. Reid, A. K. Bertram, D. O. Topping, A. Laskin, S. T. Martin, M. D. Petters, F. D. Pope  
35 510 and G. Rovelli, The viscosity of atmospherically relevant organic particles, *Nat.*  
36 511 *Commun.*, 2018, **9**, 956.
- 37 512 38 J. F. Davies and K. R. Wilson, Raman spectroscopy of isotopic water diffusion in  
38 513 ultraviscous, glassy, and gel states in aerosol by use of optical tweezers, *Anal. Chem.*,  
39 514 2016, **88**, 2361–2366.
- 40 515 39 D. J. Stewart, C. Cai, J. Nayler, T. C. Preston, J. P. Reid, U. K. Krieger, C. Marcolli and Y.  
41 516 H. Zhang, Liquid-liquid phase separation in mixed organic/inorganic single aqueous  
42 517 aerosol droplets, *J. Phys. Chem. A*, 2015, **119**, 4177–4190.
- 43 518 40 Y. Zhang, Y. Chen, A. T. Lambe, N. E. Olson, Z. Lei, R. L. Craig, Z. Zhang, A. Gold, T. B.  
44 519 Onasch, J. T. Jayne, D. R. Worsnop, C. J. Gaston, J. A. Thornton, W. Vizuete, A. P. Ault  
45 520 and J. D. Surratt, Effect of the aerosol-phase state on secondary organic aerosol formation  
46 521 from the reactive uptake of isoprene-derived epoxydiols (IEPOX), *Environ. Sci. Technol.*  
47 522 *Lett.*, 2018, **5**, 167–174.
- 48 523 41 A. L. Robinson, N. M. Donahue, M. K. Shrivastava, E. A. Weitkamp, A. M. Sage, A. P.

- 1  
2  
3 524 Grieshop, T. E. Lane, J. R. Pierce and S. N. Pandis, Rethinking organic aerosols:  
4 525 Semivolatile emissions and photochemical aging, *Science*, 2007, **315**, 1259–1262.
- 5 526 42 N. M. Donahue, A. L. Robinson, C. O. Stanier and S. N. Pandis, Coupled partitioning,  
6 527 dilution, and chemical aging of semivolatile organics, *Environ. Sci. Technol.*, 2006, **40**,  
7 528 2635–2643.
- 8  
9 529 43 E. A. Stefaniak, A. Buczynska, V. Novakovic, R. Kuduk and R. Van Grieken, Determination  
10 530 of chemical composition of individual airborne particles by SEM/EDX and micro-Raman  
11 531 spectrometry: A review, *J. Phys. Conf. Ser.*, 2009, **162**, 12019.
- 12 532 44 A. P. Ault, D. Zhao, C. J. Ebben, M. J. Tauber, F. M. Geiger, K. A. Prather and V. H.  
13 533 Grassian, Raman microspectroscopy and vibrational sum frequency generation  
14 534 spectroscopy as probes of the bulk and surface compositions of size-resolved sea spray  
15 535 aerosol particles, *Phys. Chem. Chem. Phys.*, 2013, **15**, 6206–6214.
- 16 536 45 J. M. Creamean, J. L. Axson, A. L. Bondy, R. L. Craig, N. W. May, H. Shen, M. H. Weber,  
17 537 K. A. Pratt and A. P. Ault, Changes in precipitating snow chemistry with location and  
18 538 elevation in the California Sierra Nevada, *J. Geophys. Res. - Atmos.*, 2016, **121**, 7296–  
19 539 7309.
- 20  
21 540 46 R. L. Craig, A. L. Bondy and A. P. Ault, Computer-controlled Raman microspectroscopy  
22 541 (CC-Raman): A method for the rapid characterization of individual atmospheric aerosol  
23 542 particles, *Aerosol Sci. Technol.*, 2017, **51**, 1099–1112.
- 24 543 47 C. Deng, S. D. Brooks, G. Vidaurre and D. C. O. Thornton, Using Raman microspectroscopy  
25 544 to determine chemical composition and mixing state of airborne marine aerosols over the  
26 545 Pacific Ocean, *Aerosol Sci. Technol.*, 2014, **48**, 193–206.
- 27  
28 546 48 S. Sobanska, G. Falgayrac, J. Rimetz-Planchon, E. Perdrix, C. Bremard and J. Barbillat,  
29 547 Resolving the internal structure of individual atmospheric aerosol particle by the  
30 548 combination of Atomic Force Microscopy, ESEM-EDX, Raman and ToF-SIMS imaging,  
31 549 *Microchem. J.*, 2014, **114**, 89–98.
- 32  
33 550 49 A. L. Bondy, B. Wang, A. Laskin, R. L. Craig, M. V Nhliziyo, S. B. Bertman, K. A. Pratt, P.  
34 551 B. Shepson and A. P. Ault, Inland sea spray aerosol transport and incomplete chloride  
35 552 depletion: Varying degrees of reactive processing observed during SOAS, *Environ. Sci.*  
36 553 *Technol.*, 2017, **51**, 9533–9542.
- 37  
38 554 50 H. Rosen, A. D. A. Hansen, L. Gundel and T. Novakov, Identification of the optically  
39 555 absorbing component in urban aerosols, *Appl. Opt.*, 1978, **17**, 3859–3861.
- 40 556 51 H. Rosen and T. Novakov, Raman scattering and the characterisation of atmospheric aerosol  
41 557 particles, *Nature*, 1977, **266**, 708–710.
- 42 558 52 N. P. Ileva, A. Messerer, X. Yang, R. Niessner and U. Pöschl, Raman microspectroscopic  
43 559 analysis of changes in the chemical structure and reactivity of soot in a diesel exhaust  
44 560 aftertreatment model system, *Environ. Sci. Technol.*, 2007, **41**, 3702–3707.
- 45 561 53 T. Catelani, G. Pratesi and M. Zoppi, Raman characterization of ambient airborne soot and  
46 562 associated mineral phases, *Aerosol Sci. Technol.*, 2014, **48**, 13–21.
- 47  
48 563 54 O. Laskina, M. A. Young, P. D. Kleiber and V. H. Grassian, Infrared extinction spectroscopy  
49 564 and micro-Raman spectroscopy of select components of mineral dust mixed with organic  
50 565 compounds, *J. Geophys. Res. - Atmos.*, 2013, **118**, 6593–6606.
- 51 566 55 H.-J. Jung, H.-J. Eom, H.-W. Kang, M. Moreau, S. Sobanska and C.-U. Ro, Combined use of  
52 567 quantitative ED-EPMA, Raman microspectrometry, and ATR-FTIR imaging techniques  
53 568 for the analysis of individual particles, *Analyst*, 2014, **139**, 3949–3960.
- 54  
55 569 56 S. Sobanska, H. Hwang, M. Choel, H. J. Jung, H. J. Eom, H. Kim, J. Barbillat and C. U. Ro,  
56  
57  
58  
59  
60

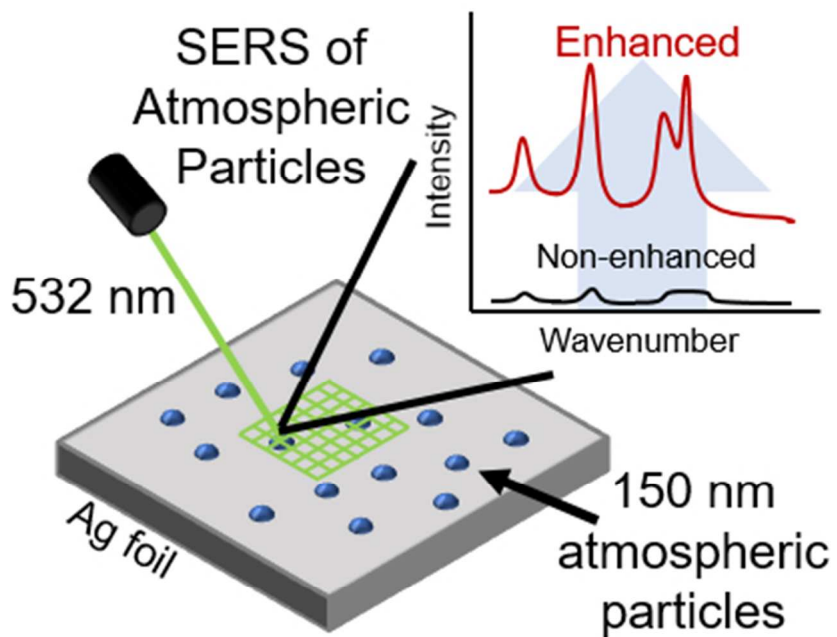


- 1  
2  
3 570 Investigation of the chemical mixing state of individual Asian dust particles by the  
4 571 combined use of electron probe X-ray microanalysis and Raman microspectrometry,  
5 572 *Anal. Chem.*, 2012, **84**, 3145–3154.
- 6 573 57 J. De Gelder, K. De Gussem, P. Vandenabeele and L. Moens, Reference database of Raman  
7 574 spectra of biological molecules, *J. Raman Spectrosc.*, 2007, **38**, 1133–1147.
- 8 575 58 R. P. McLaughlin, B. Bird and P. J. Reid, Vibrational analysis of isopropyl nitrate and  
9 576 isobutyl nitrate, *Spectrochim. Acta Part A Mol. Biomol. Spectrosc.*, 2002, **58**, 2571–2580.
- 10 577 59 A. L. Bondy, R. L. Craig, Z. Zhang, A. Gold, J. D. Surratt and A. P. Ault, Isoprene-derived  
11 578 organosulfates: Vibrational mode analysis by Raman spectroscopy, acidity-dependent  
12 579 spectral modes, and observation in individual atmospheric particles, *J. Phys. Chem. A*,  
13 580 2018, **122**, 303–315.
- 14 581 60 E. Avzianova and S. D. Brooks, Raman spectroscopy of glyoxal oligomers in aqueous  
15 582 solutions, *Spectrochim. Acta Part A Mol. Biomol. Spectrosc.*, 2013, **101**, 40–48.
- 16 583 61 M. C. Yeung and C. K. Chan, Water content and phase transitions in particles of inorganic  
17 584 and organic species and their mixtures using micro-Raman spectroscopy, *Aerosol Sci.*  
18 585 *Technol.*, 2010, **44**, 269–280.
- 19 586 62 Y. Chu, M. Sauerwein and C. K. Chan, Hygroscopic and phase transition properties of alkyl  
20 587 aminium sulfates at low relative humidities, *Phys. Chem. Chem. Phys.*, 2015, **17**, 19789–  
21 588 19796.
- 22 589 63 N. Jordanov and R. Zellner, Investigations of the hygroscopic properties of ammonium  
23 590 sulfate and mixed ammonium sulfate and glutaric acid micro droplets by means of optical  
24 591 levitation and Raman spectroscopy, *Phys. Chem. Chem. Phys.*, 2006, **8**, 2759–2764.
- 25 592 64 D. L. Bones, J. P. Reid, D. M. Lienhard and U. K. Krieger, Comparing the mechanism of  
26 593 water condensation and evaporation in glassy aerosol, *Proc. Natl. Acad. Sci.*, 2012, **109**,  
27 594 11613–11618.
- 28 595 65 A. K. Y. Lee, T. Y. Ling and C. K. Chan, Understanding hygroscopic growth and phase  
29 596 transformation of aerosols using single particle Raman spectroscopy in an electrodynamic  
30 597 balance, *Faraday Discuss.*, 2008, **137**, 245–263.
- 31 598 66 A. K. Bertram, S. T. Martin, S. J. Hanna, M. L. Smith, A. Bodsworth, Q. Chen, M. Kuwata,  
32 599 A. Liu, Y. You and S. R. Zorn, Predicting the relative humidities of liquid-liquid phase  
33 600 separation, efflorescence, and deliquescence of mixed particles of ammonium sulfate,  
34 601 organic material, and water using the organic-to-sulfate mass ratio of the particle and the  
35 602 oxygen-to-carbon ele, *Atmos. Chem. Phys.*, 2011, **11**, 10995–11006.
- 36 603 67 Q. Zhou, S.-F. Pang, Y. Wang, J.-B. Ma and Y.-H. Zhang, Confocal Raman studies of the  
37 604 evolution of the physical state of mixed phthalic acid/ammonium sulfate aerosol droplets  
38 605 and the effect of substrates, *J. Phys. Chem. B*, 2014, **118**, 6198–6205.
- 39 606 68 V. G. Ciobanu, C. Marcolli, U. K. Krieger, U. Weers and T. Peter, Liquid–liquid phase  
40 607 separation in mixed organic/inorganic aerosol particles, *J. Phys. Chem. A*, 2009, **113**,  
41 608 10966–10978.
- 42 609 69 A. P. Ault, T. L. Guasco, J. Baltrusaitis, O. S. Ryder, J. V Trueblood, D. B. Collins, M. J.  
43 610 Ruppel, L. A. Cuadra-Rodriguez, K. A. Prather and V. H. Grassian, Heterogeneous  
44 611 reactivity of nitric acid with nascent sea spray aerosol: Large differences observed  
45 612 between and within individual particles, *J. Phys. Chem. Lett.*, 2014, **5**, 2493–2500.
- 46 613 70 A. K. Y. Lee and C. K. Chan, Single particle Raman spectroscopy for investigating  
47 614 atmospheric heterogeneous reactions of organic aerosols, *Atmos. Environ.*, 2007, **41**,  
48 615 4611–4621.

- 1  
2  
3 616 71 K. J. Baustian, D. J. Cziczo, M. E. Wise, K. A. Pratt, G. Kulkarni, A. G. Hallar and M. A.  
4 617 Tolbert, Importance of aerosol composition, mixing state, and morphology for  
5 618 heterogeneous ice nucleation: A combined field and laboratory approach, *J. Geophys.*  
6 619 *Res.*, 2012, **117**, D06217.
- 8 620 72 J. D. Rindelaub, R. L. Craig, L. Nandy, A. L. Bondy, C. S. Dutcher, P. B. Shepson and A. P.  
9 621 Ault, Direct measurement of pH in individual particles via Raman microspectroscopy and  
10 622 variation in acidity with relative humidity, *J. Phys. Chem. A*, 2016, **120**, 911–917.
- 11 623 73 R. L. Craig, L. Nandy, J. L. Axson, C. S. Dutcher and A. P. Ault, Spectroscopic  
12 624 determination of aerosol pH from acid–base equilibria in inorganic, organic, and mixed  
13 625 systems, *J. Phys. Chem. A*, 2017, **121**, 5690–5699.
- 15 626 74 O. Laskina, H. S. Morris, J. R. Grandquist, Z. Qin, E. A. Stone, A. V. Tivanski and V. H.  
16 627 Grassian, Size matters in the water uptake and hygroscopic growth of atmospherically  
17 628 relevant multicomponent aerosol particles, *J. Phys. Chem. A*, 2015, **119**, 4489–4497.
- 18 629 75 S. Schlucker, Surface-Enhanced Raman Spectroscopy: Concepts and Chemical Applications,  
19 630 *Angew. Chemie-International Ed.*, 2014, **53**, 4756–4795.
- 20 631 76 K. Kneipp, Y. Wang, H. Kneipp, L. T. Perelman, I. Itzkan, R. Dasari and M. S. Feld, Single  
21 632 molecule detection using surface-enhanced Raman scattering (SERS), *Phys. Rev. Lett.*,  
22 633 1997, **78**, 1667–1670.
- 24 634 77 E. L. Keller, N. C. Brandt, A. A. Cassabaum and R. R. Frontiera, Ultrafast surface-enhanced  
25 635 Raman spectroscopy, *Analyst*, 2015, **140**, 4922–4931.
- 26 636 78 S. L. Kleinman, R. R. Frontiera, A. I. Henry, J. A. Dieringer and R. P. Van Duyne, Creating,  
27 637 characterizing, and controlling chemistry with SERS hot spots, *Phys. Chem. Chem. Phys.*,  
28 638 2013, **15**, 21–36.
- 29 639 79 S. Nie and S. R. Emory, Probing single molecules and single nanoparticles by surface-  
30 640 enhanced Raman scattering, *Science.*, 1997, **275**, 1102–1106.
- 32 641 80 B. Sharma, R. R. Frontiera, A.-I. Henry, E. Ringe and R. P. Van Duyne, SERS: Materials,  
33 642 applications, and the future, *Mater. Today*, 2012, **15**, 16–25.
- 34 643 81 B. Sharma, M. F. Cardinal, S. L. Kleinman, N. G. Greeneltch, R. R. Frontiera, M. G. Blaber,  
35 644 G. C. Schatz and R. P. Van Duyne, High-performance SERS substrates: Advances and  
36 645 challenges, *MRS Bull.*, 2013, **38**, 615–624.
- 38 646 82 M. C. S. Pierre, P. M. Mackie, M. Roca and A. J. Haes, Correlating molecular surface  
39 647 coverage and solution-phase nanoparticle concentration to surface-enhanced Raman  
40 648 scattering intensities, *J. Phys. Chem. C*, 2011, **115**, 18511–18517.
- 41 649 83 A. B. Zrimsek, N. Chiang, M. Mattei, S. Zaleski, M. O. McAnally, C. T. Chapman, A. I.  
42 650 Henry, G. C. Schatz and R. P. Van Duyne, Single-molecule chemistry with surface- and  
43 651 tip-enhanced Raman spectroscopy, *Chem. Rev.*, 2017, **117**, 7583–7613.
- 45 652 84 M. J. Ayora, L. Ballesteros, R. Perez, A. Ruperez and J. J. Laserna, Detection of atmospheric  
46 653 contaminants in aerosols by surface-enhanced Raman spectrometry, *Anal. Chim. Acta*,  
47 654 1997, **355**, 15–21.
- 48 655 85 A. Sengupta, M. L. Laucks, N. Dildine, E. Drapala and E. J. Davis, Bioaerosol  
49 656 characterization of surface-enhanced Raman spectroscopy (SERS), *Aerosol Sci.*, 2005,  
50 657 **36**, 651–664.
- 51 658 86 K. Schwarzmeier, M. Knauer, N. P. Ileva, R. Niessner and C. Haisch, Bioaerosol analysis  
52 659 based on a label-free microarray readout method using surface-enhanced Raman  
53 660 scattering, *Anal. Bioanal. Chem.*, 2013, **405**, 5387–5392.
- 54 661 87 R. L. Craig, A. L. Bondy and A. P. Ault, Surface enhanced Raman spectroscopy enables  
55 662

- 662 observations of previously undetectable secondary organic aerosol components at the  
663 individual particle level, *Anal. Chem.*, 2015, **87**, 7510–7514.
- 664 88 Y. Fu, C. Kuppe, V. K. Valev, H. Fu, L. Zhang and J. Chen, Surface-enhanced Raman  
665 spectroscopy: A facile and rapid method for the chemical component study of individual  
666 atmospheric aerosol, *Environ. Sci. Technol.*, 2017, **51**, 6260–6267.
- 667 89 J. Ofner, T. Deckert-Gaudig, K. A. Kamilli, A. Held, H. Lohninger, V. Deckert and B. Lendl,  
668 Tip-enhanced Raman spectroscopy of atmospherically relevant aerosol nanoparticles,  
669 *Anal. Chem.*, 2016, **88**, 9766–9772.
- 670 90 M. Gen and C. K. Chan, Electrospray surface-enhanced Raman spectroscopy (ES-SERS) for  
671 probing surface chemical compositions of atmospherically relevant particles, *Atmos.*  
672 *Chem. Phys.*, 2017, **17**, 14025–14037.
- 673 91 V. Sivaprakasam, M. B. Hart and J. D. Eversole, Surface enhanced Raman spectroscopy of  
674 individual suspended aerosol particles, *J. Phys. Chem. C*, 2017, **121**, 22326–22334.
- 675 92 N. Leopold and B. Lendl, A new method for fast preparation of highly surface-enhanced  
676 Raman scattering (SERS) active silver colloids at room temperature by reduction of silver  
677 nitrate with hydroxylamine hydrochloride, *J. Phys. Chem. B*, 2003, **107**, 5723–5727.
- 678 93 J. L. Axson, D. I. Stark, A. L. Bondy, S. S. Capracotta, A. D. Maynard, M. A. Philbert, I. L.  
679 Bergin and A. P. Ault, Rapid kinetics of size and pH-dependent dissolution and  
680 aggregation of silver nanoparticles in simulated gastric fluid, *J. Phys. Chem. C*, 2015,  
681 **119**, 20632–20641.
- 682 94 I. L. Bergin, L. A. Wilding, M. Morishita, K. Walacavage, A. P. Ault, J. L. Axson, D. I.  
683 Stark, S. A. Hashway, S. S. Capracotta, P. R. Leroueil, A. D. Maynard and M. A.  
684 Philbert, Effects of particle size and coating on toxicologic parameters, fecal elimination  
685 kinetics and tissue distribution of acutely ingested silver nanoparticles in a mouse model,  
686 *Nanotoxicology*, 2016, **10**, 352–360.
- 687 95 A. P. Ault, D. I. Stark, J. L. Axson, J. N. Keeney, A. D. Maynard, I. L. Bergin and M. A.  
688 Philbert, Protein corona-induced modification of silver nanoparticle aggregation in  
689 simulated gastric fluid, *Environ. Sci. Nano*, 2016, **3**, 1510–1520.
- 690 96 P. A. Schueler, J. T. Ives, F. DeLaCroix, W. B. Lacy, P. A. Becker, J. Li, K. D. Caldwell, B.  
691 Drake and J. M. Harris, Physical structure, optical resonance, and surface-enhanced  
692 Raman scattering of silver-island films on suspended polymer latex particles, *Anal.*  
693 *Chem.*, 1993, **65**, 3177–3186.
- 694 97 E. C. Le Ru, E. Blackie, M. Meyer and P. G. Etchegoin, Surface enhanced Raman scattering  
695 enhancement factors: A comprehensive study, *J. Phys. Chem. C*, 2007, **111**, 13794–  
696 13803.
- 697 98 P. Larkin, *Infrared and Raman Spectroscopy; Principles and Spectral Interpretation*,  
698 Elsevier, Waltham, MA, 2011.
- 699 99 B. Jasse, R. S. Chao and J. L. Koenig, Laser Raman scattering in uniaxially oriented atactic  
700 polystyrene, *J. Polym. Sci. Polym. Phys. Ed.*, 1978, **16**, 2157–2169.
- 701 100 W. M. Sears, J. L. Hunt and J. R. Stevens, Raman scattering from polymerizing styrene.  
702 I. Vibrational mode analysis, *J. Chem. Phys.*, 1981, **75**, 1589–1598.
- 703 101 A. Laskin, M. K. Gilles, D. A. Knopf, B. Wang and S. China, Progress in the analysis of  
704 complex atmospheric particles, *Annu. Rev. Anal. Chem.*, 2016, **9**, 117–143.
- 705 102 P. Venkateswarlu, H. D. Bist and Y. S. Jain, Laser excited Raman spectrum of  
706 ammonium sulfate single crystal, *J. Raman Spectrosc.*, 1975, **3**, 143–151.
- 707 103 P. V. Jentsch, B. Kampe, V. Ciobota, P. Roesch and J. Popp, Inorganic salts in

- 1  
2  
3 708 atmospheric particulate matter: Raman spectroscopy as an analytical tool, *Spectrochim.*  
4 709 *Acta Part A Mol. Biomol. Spectrosc.*, 2013, **115**, 697–708.  
5 710 104 D. L. Rousseau, R. E. Miller and G. E. Leroi, Raman spectrum of crystalline sodium  
6 711 nitrate, *J. Chem. Phys.*, 1968, **48**, 3409-3413.  
7 712 105 S. Gajaraj, C. Fan, M. Lin and Z. Hu, Quantitative detection of nitrate in water and  
8 713 wastewater by surface-enhanced Raman spectroscopy, *Environ. Monit. Assess.*, 2013,  
9 714 **185**, 5673–5681.  
10 715 106 K. H. Michaelian, The Raman spectrum of kaolinite #9 at 21 C, *Can. J. Chem. Can.*  
11 716 *Chim.*, 1986, **64**, 285–289.  
12 717 107 R. L. Frost, Fourier transform Raman spectroscopy of kaolinite, dickite, and halloysite,  
13 718 *Clays Clay Miner.*, 1995, **43**, 191–195.  
14 719 108 R. L. Frost, T. Thu Ha and J. Kristof, FT-Raman spectroscopy of the lattice region of  
15 720 kaolinite and its intercalates, *Vib. Spectrosc.*, 1997, **13**, 175–186.  
16 721 109 J. de Villepin and A. Novak, Vibrational spectra of and isotope effect in hydrogen  
17 722 bonded potassium hydrogen oxalate, *Spectrosc. Lett.*, 1971, **4**, 1–8.  
18 723 110 J. L. Koenig and A. C. Angood, Raman spectra of poly(ethylene glycols) in solution, *J.*  
19 724 *Polym. Sci. Part A-2*, 1970, **8**, 1787-.  
20 725  
21 726  
22  
23  
24  
25  
26  
27  
28  
29  
30  
31  
32  
33  
34  
35  
36  
37  
38  
39  
40  
41  
42  
43  
44  
45  
46  
47  
48  
49  
50  
51  
52  
53  
54  
55  
56  
57  
58  
59  
60



79x60mm (150 x 150 DPI)

1  
2  
3  
4  
5  
6  
7  
8  
9  
10  
11  
12  
13  
14  
15  
16  
17  
18  
19  
20  
21  
22  
23  
24  
25  
26  
27  
28  
29  
30  
31  
32  
33  
34  
35  
36  
37  
38  
39  
40  
41  
42  
43  
44  
45  
46  
47  
48  
49  
50  
51  
52  
53  
54  
55  
56  
57  
58  
59  
60